CHINESE OPTICS LETTERS

Vol. 22, No. 3 | March 2024

Ultra-compact and broadband polarization-insensitive mode-order converting power splitter

Haoqi Chen (陈浩琪)[1], Runkui Yao (姚润葵)[1], Pengjun Wang (汪鹏君)[2*], Qiang Fu (符 强)[3], Weiwei Chen (陈伟伟)[1**], Shixun Dai (戴世勋)[1,4], Dejun Kong (孔德军)[1], Jian Lin (林 健)[1], Tao Jin (金 涛)[1], Jun Li (李 军)[1], Tingge Dai (戴庭舸)[5], and Jianyi Yang (杨建义)[5]

[1] Faculty of Electrical Engineering and Computer Science, Ningbo University, Ningbo 315211, China

[2] College of Electrical and Electronic Engineering, Wenzhou University, Wenzhou 325035, China

[3] College of Science and Technology, Ningbo University, Ningbo 315211, China

[4] Laboratory of Infrared Materials and Devices, The Research Institute of Advanced Technologies, Ningbo University, Ningbo 315211, China

[5] Department of Information Science and Electronics Engineering, Zhejiang University, Hangzhou 310027, China

*Corresponding author: wangpengjun@wzu.edu.cn

**Corresponding author: chenweiwei@nbu.edu.cn

Received August 24, 2023 | Accepted October 19, 2023 | Posted Online March 19, 2024

A polarization-insensitive mode-order converting power splitter using a pixelated region is presented and investigated in this paper. As TE_0 and TM_0 modes are injected into the input port, they are converted into TE_1 and TM_1 modes, which evenly come out from the two output ports. The finite-difference time-domain method and direct-binary-search optimization algorithm are utilized to optimize structural parameters of the pixelated region to attain small insertion loss, low crosstalk, wide bandwidth, excellent power uniformity, polarization-insensitive property, and compact size. Experimental results reveal that the insertion loss, crosstalk, and power uniformity of the fabricated device at 1550 nm are 0.57, −19.67, and 0.094 dB in the case of TE polarization, while in the TM polarization, the relevant insertion loss, crosstalk, and power uniformity are 0.57, −19.40, and 0.11 dB. Within a wavelength range from 1520 to 1600 nm, for the fabricated device working at TE polarization, the insertion loss, crosstalk, and power uniformity are lower than 1.39, −17.64, and 0.14 dB. In the case of TM polarization, we achieved an insertion loss, crosstalk, and power uniformity less than 1.23, −17.62, and 0.14 dB.

Keywords: integrated optics; optical waveguide; polarization-insensitive property; mode-order converting power splitter.
DOI: 10.3788/COL202422.031301

1. Introduction

Due to their CMOS-compatible, high-speed, and broad-bandwidth characteristics, silicon-based optical interconnects have been deemed as a promising solution to meet the rising demand for high-capacity transmission communication[1,2]. For example, a variety of techniques, such as wavelength-division multiplexing, mode-division multiplexing (MDM), and polarization-division multiplexing, have been exploited to implement capacity expansion. In particular, MDM, where each guided mode is regarded as an independent data channel, giving a new dimension to enlarge the transmission capacity further, is attracting much attention[3].

To date, various sorts of elements such as multimode waveguide bends, multimode optical filters, multimode waveguide crossings, multimode optical switches, and mode (de)multiplexers, have been introduced to realize on-chip MDM transmission. Mode-order converters transforming the low-order (high-order) modes to the high-order (low-order) modes and optical power splitters splitting or combining guided modes also play important roles in MDM transmission. In recent years, silicon mode-order converters based on different structures, including the planar metasurfaces[4], dielectric slots[5], asymmetric tapers and subwavelength gratings (SWGs)[6], photonic crystal waveguides[7], and SWGs assisted with Mach–Zehnder interferometers[8], have been reported. Similarly, silicon-based optical power splitters using various structures, including a multimode interference (MMI) coupler[9], asymmetrical directional couplers and a Y-branch[10], a photonic crystal-like structure[11,12], a subwavelength grating structure[13], and an adiabatic coupler[14], have also been presented. However, to achieve the mode converting and splitting operations simultaneously, it is often necessary to cascade the mode-order converter with the optical power splitter, resulting in a large footprint.

Previously, a design of a mode-order converting power splitter using SWGs assisted with an MMI coupler has been proposed and analyzed at the mid-infrared wavelength[15]. It works at transverse-electric (TE) polarization. To the best of our knowledge, the experimental demonstrations of mode-order converting power splitters have never before been discussed. In addition, a remarkable polarization dependence can be produced on account of a large refractive index contrast in the silicon-on-insulator (SOI) platform. Consequently, polarization-insensitive mode-order converting power splitters (PIMCPSs) are urgently needed.

In this paper, we present, design, and experimentally demonstrate a PIMCPS using a pixelated region, which is optimized by employing the finite-difference time-domain (FDTD) method and direct-binary-search (DBS) optimization algorithm to realize excellent power uniformity (PU), a small insertion loss (IL), a wide bandwidth (BW), low crosstalk (CT), a compact footprint, and polarization-insensitive properties. Experimental results show that the length of the pixelated region is only 4 μm. In TE polarization, the CT, IL, and PU of the fabricated PIMCPS are less than-17.64 dB, 1.39 dB, and 0.14 dB within a BW from 1520 to 1600 nm, while in transverse-magnetic (TM) polarization, the corresponding CT, IL, and PU are smaller than −17.62 dB, 1.23 dB, and 0.14 dB within a wavelength range from 1520 to 1600 nm.

2. Principle and Design

Figure 1(a) describes a schematic drawing of our introduced PIMCPS consisting of an input strip waveguide, a pixelated region, and two output strip waveguides. This device is designed to be axisymmetric along line A–A′. The widths of the input waveguide and the two output waveguides are labeled as W_1, W_2, and W_3, which are chosen as $W_1 = W_2 = W_3 = 1.3\,\mu m$ to support the TE_0, TM_0, TE_1, and TM_1 modes. The spacing between the two output waveguides is denoted by G_0, which is set as $G_0 = 1.2\,\mu m$. The length of the pixelated region is marked as L_0, which is chosen to be 4 μm. In the pixelated region, there are 19×18 identical pixels. Each pixel's shape is a square of $0.2\,\mu m \times 0.2\,\mu m$ with a central circular hole, where the diameter D_0 is 100 nm and its logic state can be "1" or "0", standing for the hole filled with SiO_2 or Si. The cross-sectional view of the pixelated region is illustrated in Fig. 1(b). The thickness H_s of the silicon waveguide is 220 nm. By defining the logic states of the pixels to tune the refractive index distribution and control the behavior of the optical field, the input TE_0 (TM_0) mode from the In port would be transformed into the TE_1 (TM_1) mode after passing through the pixelated region, and the TE_1 (TM_1) mode uniformly exits from the two output ports O_1 and O_2. In order to convert and split the targeted modes within a compact length more efficiently, the DBS optimization algorithm and the FDTD method are employed to optimize each pixel's logic state. The optimization figure of merit (FoM) is written as

$$\begin{aligned} \mathrm{FoM} = \alpha \cdot (P_{\mathrm{TE0-O1-TE1}} + P_{\mathrm{TE1-O2-TE1}}) + (1-\alpha) \\ \cdot (P_{\mathrm{TM0-O1-TM1}} + P_{\mathrm{TM0-O2-TM1}}), \end{aligned} \tag{1}$$

where α stands for the weight coefficient that is set to be 0.5 in this simulation, and $P_{\mathrm{TE0(TM0)-O1-TE1(TM1)}}$ and $P_{\mathrm{TE0(TM0)-O2-TE1(TM1)}}$ represent the optical power of the TE_1 (TM_1) mode received from the output ports O_1 and O_2 as the TE_0 (TM_0) mode is launched into the In port. The optimization steps involved are described as follows.

(1) Due to its axisymmetric structure, it can be simplified to optimize 19×9 pixels. Set their logic states to be 0 and assign the variables n and m to be $n = 1$ and $m = 1$.
(2) Implement FDTD simulation and calculate the corresponding FoM.

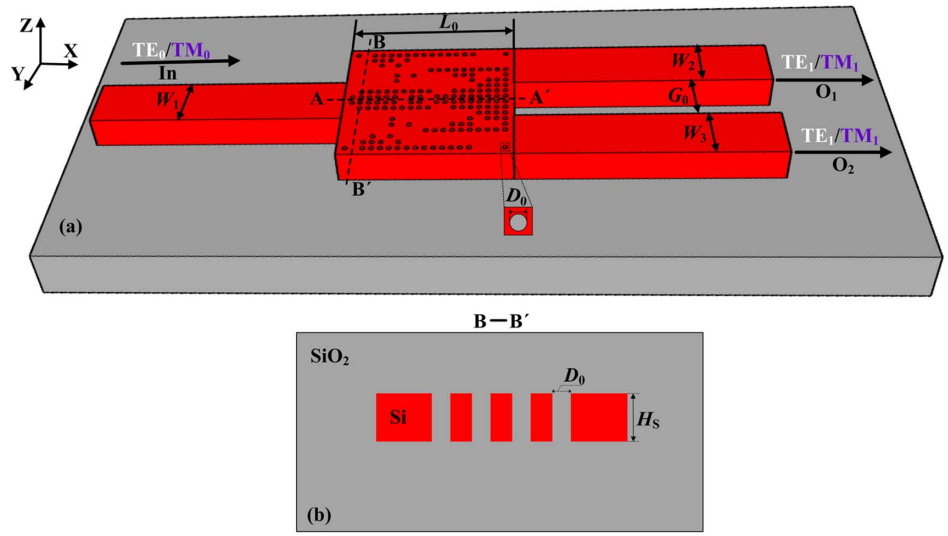

Fig. 1. (a) Schematic drawing of our introduced PIMCPS. (b) Cross-sectional view of the pixelated region along line B-B′.

(3) Choose the nth pixel, alter the logic state, implement FDTD simulation, and recalculate the FoM.
(4) If the FoM is improved, then save the current logic state. Otherwise, flip its logic state.
(5) When $n > 171$ is met, assign the variables n and m to be $n = 1$ and $m = m + 1$. Otherwise, the variable n is updated to $n = n + 1$ and return to step (3).
(6) When $m > 10$ or FoM > 0.99 is met, terminate the optimization. Otherwise, return to step (3).

According to the above optimization steps, it takes approximately 36 hours to realize the optimized logic states of the pixels by adopting a computer with a 16-core central processing unit (Inter Core i7-10700K).

The simulated light propagation in the optimized PIMCPS is shown in Fig. 2. As the TE_0 and TM_0 modes are injected into the In port, they are converted into TE_1 and TM_1 modes. Then, the TE_1 and TM_1 modes are evenly separated and come out from the two output ports O_1 and O_2. In other words, the corresponding functionality of the optimized PIMCPS can be executed well.

Figure 3 shows the CT, IL, and PU of our optimized PIMCPS as a function of the wavelength. As seen in Fig. 3, within a BW from 1518 to 1611 nm, for the optimized PIMCPS in TE polarization, CT < -19.57 dB, IL < 0.49 dB, PU < 0.004 are obtained, while in the case of the optimized PIMCPS in TM polarization, CT < -19.16 dB, IL < 0.60 dB, and PU < 0.0041 are achieved. At 1550 nm, in TE polarization, the designed PIMCPS can have a CT of -21.82 dB, an IL of 0.28 dB, and a PU of 0.00308, while in TM polarization, the CT, IL, and PU are -21.76 dB, 0.45 dB, and 0.00028 dB, respectively. The corresponding IL, CT, and PU are defined as

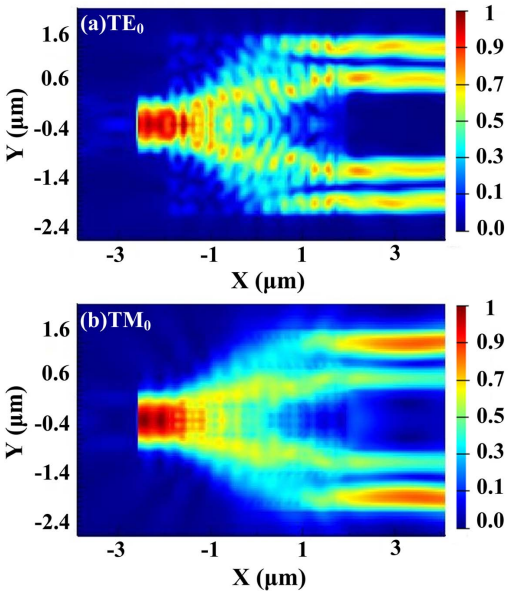

Fig. 2. Simulated light propagation in the optimized PIMCPS with input (a) TE_0 or (b) TM_0 mode.

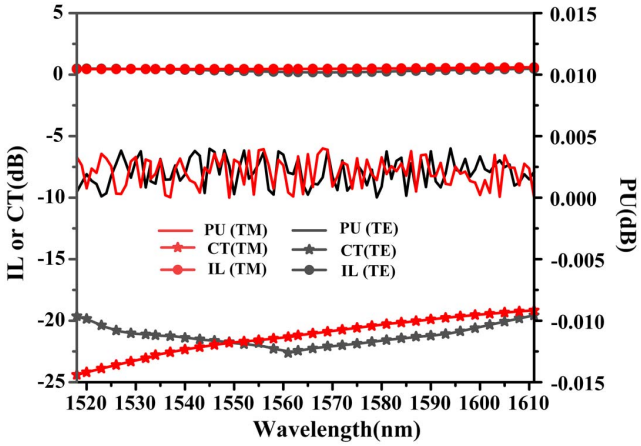

Fig. 3. CT, IL, and PU of the designed PIMCPS as a function of the wavelength.

$$\mathrm{IL}_{\mathrm{TE(TM)}} = -10 \times \log\left(\frac{P_{\mathrm{TE0(TM0)\text{-}O1\text{-}TE1(TM1)}} + P_{\mathrm{TE0(TM0)\text{-}O2\text{-}TE1(TM1)}}}{P_{\mathrm{In\text{-}TE0(TM0)}}}\right), \tag{2}$$

$$\mathrm{CT}_{\mathrm{TE(TM)}} = 10 \times \log\left(\frac{P_{\mathrm{O1\text{-}other}} + P_{\mathrm{O2\text{-}other}}}{P_{\mathrm{TE0(TM0)\text{-}O1\text{-}TE1(TM1)}} + P_{\mathrm{TE0(TM0)\text{-}O2\text{-}TE1(TM1)}}}\right), \tag{3}$$

$$\mathrm{PU}_{\mathrm{TE(TM)}} = -10 \times \log\left(\frac{\min(P_{\mathrm{TE0(TM0)\text{-}O1\text{-}TE1(TM1)}}, P_{\mathrm{TE0(TM0)\text{-}O2\text{-}TE1(TM1)}})}{\max(P_{\mathrm{TE0(TM0)\text{-}O1\text{-}TE1(TM1)}}, P_{\mathrm{TE0(TM0)\text{-}O2\text{-}TE1(TM1)}})}\right), \tag{4}$$

where $P_{\mathrm{In\text{-}TE0(TM0)}}$ is the optical power of the TE_0 (TM_0) mode input into the In port, and $P_{\mathrm{O1\text{-}other}}$ and $P_{\mathrm{O2\text{-}other}}$ are the optical power of the undesired modes received from the ports O_1 and O_2 as the TE_0 (TM_0) mode is launched into the input In port.

Figure 4 depicts the IL, CT, and PU of our optimized PIMCPS as a function of the waveguide width variation ΔW and the diameter variation ΔD at 1550 nm. As seen in Fig. 4, different values of ΔW and ΔD have an impact on the IL, CT, and PU of the designed PIMCPS. As ΔW varies from -20 to 20 nm and ΔD is set to be 20 nm, 15 nm, 10 nm, 0 nm, -10 nm, -15 nm, or -20 nm, IL < 0.89 dB, CT < -15.71 dB, and PU < 0.010 dB are realized in TM polarization, while in TE polarization, the calculated IL, CT, and PU are less than 1.62 dB, -16.68 dB, and 0.097 dB, respectively.

3. Fabrication and Characterization

By taking advantage of electron-beam lithography, two-step inductively coupled plasma dry etching, and plasma-enhanced chemical vapor deposition processes, we fabricated the optimized PIMCPSs. Figure 5 depicts the microscopic image

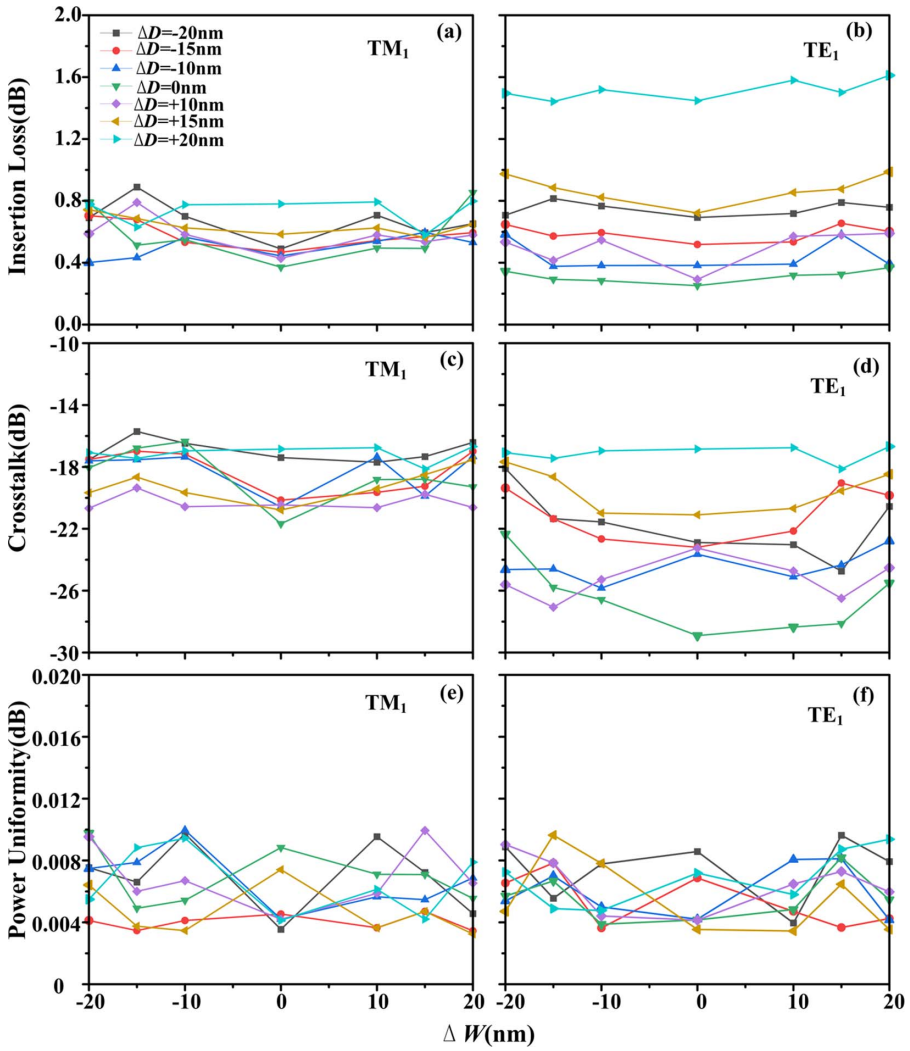

Fig. 4. (a), (b) IL, (c), (d) CT, and (e), (f) PU of the designed PIMCPS changing with ΔW and ΔD when the output modes are TM_1 and TE_1 modes.

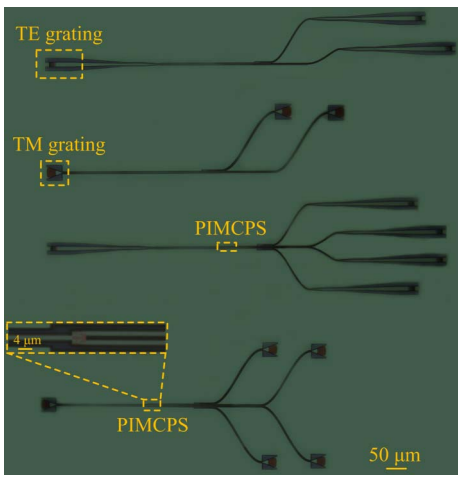

Fig. 5. Microscopic image of the fabricated PIMCPSs and two-mode demultiplexers.

of the fabricated PIMCPSs and the relevant two-mode demultiplexers.

A tunable semiconductor laser (SANTEC TSL-550) and a multi-port optical powermeter (SANTEC MPM-210) are employed for characterizing the performance of the fabricated PIMCPSs. To couple the TM-polarized or the TE-polarized light beam into and out of the fabricated devices, the focusing grating coupler or photonic crystal structure is adopted, respectively. The measured transmission of the presented PIMCPS would be normalized by subtracting the transmission of the relevant two-mode demultiplexer. Figure 6 illustrates the measured CT, IL, and PU of the fabricated PIMCPS as a function of the wavelength. Note that in Fig. 6, at 1550 nm, the measured IL, CT, and PU are respectively 0.57 dB, −19.67 dB, and 0.094 dB in TE polarization. In TM polarization, the measured IL, CT, and PU are 0.57 dB, −19.40 dB, and 0.11 dB, respectively. Within a BW from 1520 to 1600 nm, in TE polarization, the measured IL, CT, and PU are smaller than 1.39 dB, −17.64 dB, and 0.14 dB, respectively, while in TM polarization, the measured IL, CT, and PU are lower than 1.23 dB, −17.62 dB,

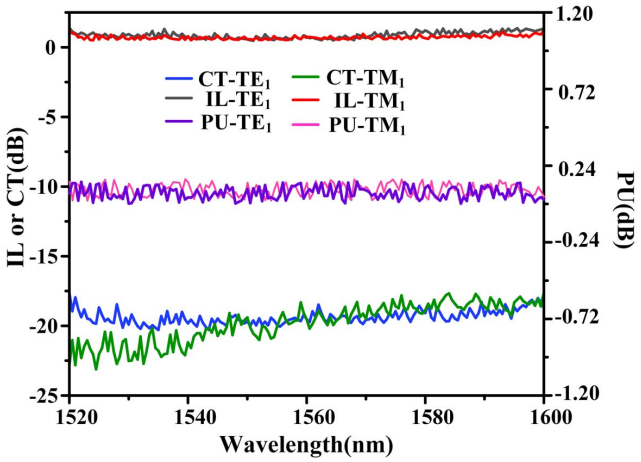

Fig. 6. Measured CT, IL, and PU of the fabricated PIMCPS as a function of the wavelength.

and 0.14 dB, respectively. The measured IL, CT, PU, and BW are also slightly worse than that in the simulation. The reasons are described below.

On the one hand, the actual fabricated waveguide width and diameter could deviate from the optimum ones in the simulation on different levels, causing the slight deteriorations of IL, CT, and PU. On the other hand, the BW obtained from the measurement is not as wide as the one in the simulation owing to the limitations of the light source used. Table 1 lists the performance of the fabricated polarization-insensitive mode-order converters (PIMOCs)[4,9], polarization-insensitive power splitters (PIPSs)[12,14], and polarization-insensitive mode-order converting power splitter. As illustrated in Table 1, compared with other devices, our PIMCPS can have a compact size, a broad BW, a relatively small IL, a low CT, and an excellent PU. In the future, high-quality and high-accuracy fabrication processes could be used to further enhance the performance of our proposed PIMCPS.

4. Conclusion

In conclusion, a PIMCPS using a pixelated region has been proposed, designed, and experimentally demonstrated. The DBS algorithm and FDTD method are employed to optimize the structural parameters of the pixelated region to achieve polarization-insensitive property, compact footprint, wide BW, small IL, low CT, and excellent PU. Measurement results reveal that, for the fabricated PIMCPS at 1550 nm, the CT, IL, and PU are −19.67 dB, 0.57 dB, and 0.094 dB, respectively, in TE polarization, while in TM polarization, the CT, IL, and PU are −19.40 dB, 0.57 dB, and 0.11 dB, respectively. Within a wavelength range from 1520 to 1600 nm, the CT, IL, and PU of the fabricated PIMCPS working at TE polarization are less than −17.64 dB, 1.39 dB, and 0.14 dB. For the fabricated PIMCPS working at TM polarization, the CT, IL, and PU are lower than −17.62 dB, 1.23 dB, and 0.14 dB. The length of the pixelated region is only 4 μm. With the above-mentioned characteristics, our introduced PIMCPS provides an attractive option for constructing an on-chip MDM transmission system.

Acknowledgements

This work was supported by the National Natural Science Foundation of China (Nos. 62275134, 62234008, and 61875098), the Zhejiang Provincial Natural Science Foundation (Nos. LY20F050003 and LY20F050001), the Youth Science and Technology Innovation Leading Talent Project of Ningbo (No. 2023QL003), the Natural Science Foundation of Ningbo (Nos. 2022J099 and 202003N4159), and the K. C. Wong Magna Fund in Ningbo University.

References

1. A. H. Atabaki, S. Moazeni, F. Pavanello, *et al.*, "Integrating photonics with silicon nanoelectronics for the next generation of systems on a chip," Nature **556**, 349 (2018).
2. A. Rahim, T. Spuesens, R. Baets, *et al.*, "Open-access silicon photonics: current status and emerging initiatives," Proc. IEEE **106**, 2313 (2018).
3. L.-W. Luo, N. Ophir, C. P. Chen, *et al.*, "WDM-compatible mode-division multiplexing on a silicon chip," Nat. Commun. **5**, 3069 (2014).
4. H. Jia, H. Chen, J. Yang, *et al.*, "Ultra-compact dual-polarization silicon mode-order converter," Opt. Lett. **44**, 4179 (2019).
5. Y. Zhao, X. Guo, Y. Zhang, *et al.*, "Ultra-compact silicon mode-order converters based on dielectric slots," Opt. Lett. **45**, 3797 (2020).

Table 1. Performance Comparison of the Proposed PIMCPS, the Reported PIMOCs, and the PIPSs.

			Measurement			
Refs.	Size (μm)	Inputs/Outputs	BW (nm)	IL (dB)	CT (dB)	PU (dB)
[4]	4	TE_0, TE_1/TM_0, TM_1	40	< 2.3	< −11.5	-
[9]	18.4	TE_0, TE_1/TM_0, TM_1	80	< 1.59	< −15.6	-
[12]	6	TE_1, TE_1/TM_1, TM_1	40	< 4.5	< −15	0.4
[14]	1600	TE_1, TE_1/TM_1, TM_1	70	< 0.68	< −15.8	< 0.8
This work	4	TE_0, TE_1/TM_0, TM_1	80	< 1.39	< −17.6	0.14

6. Z. Guo, S. Wu, and J. Xiao, "Compact and flexible mode-order converter based on mode transitions composed of asymmetric tapers and subwavelength gratings," J. Lightwave Technol. **39**, 5563 (2021).
7. L. H. Frandsen, Y. Elesin, L. F. Frellsen, *et al.*, "Topology optimized mode conversion in a photonic crystal waveguide fabricated in silicon-on-insulator material," Opt. Express **22**, 8525 (2014).
8. Z. Yuan, Y. Wang, M. Chen, *et al.*, "Ultra-broadband silicon dual-polarization mode-order converter assisted with subwavelength gratings," in *European Conference and Exhibition on Optical Communication* (Optica Publishing Group, 2022), paper We3E.2.
9. R. Liu, L. Lu, P. Zhang, *et al.*, "Integrated dual-mode 3-dB power splitter based on multimode interference coupler," IEEE Photon. Technol. Lett. **32**, 883 (2020).
10. H. Xu and Y. Shi, "Ultra-broadband dual-mode 3 dB power splitter based on a Y-junction assisted with mode converters," Opt. Lett. **41**, 5047 (2016).
11. W. Chang, X. Ren, Y. Ao, *et al.*, "Inverse design and demonstration of an ultracompact broadband dual-mode 3 dB power splitter," Opt. Express **26**, 24135 (2018).
12. Y. Liu, Z. Wang, Y. Liu, *et al.*, "Ultra-compact mode-division multiplexed photonic integrated circuit for dual polarizations," J. Lightwave Technol. **39**, 5925 (2021).
13. H. Shiran, G. Zhang, and O. Liboiron-Ladouceur, "Dual-mode broadband compact 2 × 2 optical power splitter using sub-wavelength metamaterial structures," Opt. Express **29**, 23864 (2021).
14. H. Xu, G. Zhang, K. H. R. Mojaver, *et al.*, "Broadband polarization/mode insensitive 3-dB optical coupler for silicon photonic switches," Opt. Express **31**, 14068 (2023).
15. Z. Guo and J. Xiao, "Ultracompact mode-order converting power splitter for mid-infrared wavelengths using an MMI coupler embedded with oblique subwavelength grating wires," Opt. Commun. **488**, 126850 (2021).